ELSEVIER

Fusion Engineering and Design 28 (1995) 492–503

Fusion Engineering and Design

# Characterization of TFTR shielding penetrations of ITER relevance in D–T neutron field

Anil Kumar [a], Mohamed A. Abdou [a], H.W. Kugel [b]

[a] *School of Engineering and Applied Science, University of California at Los Angeles, Los Angeles, CA 90095, USA*
[b] *Princeton Plasma Physics Laboratory, Princeton University, Princeton, NJ 08543, USA*

**Abstract**

D–T phase of TFTR began with trace tritium discharges in mid-November 1993. The availability of high D–T fusion neutron yields at TFTR has provided a unique opportunity to characterize tokamak fusion reactor shielding–penetration geometries of relevance to ITER. It was undertaken to characterize neutron energy spectra near three different kinds of penetrations on walls of TFTR test cell. Thirteen foils each were irradiated on seven locations. The saturation activities have been obtained and are discussed with a view to characterizing the neutron energy spectra. Also, unfolded spectra have been utilized to estimate dose equivalents for the same locations. These types of measurements are potentially useful for validating calculational methods and meeting fusion reactor licensing requirements.

## 1. Introduction

Engineering design activities of International Thermonuclear Experimental Reactor (ITER) are in progress. It is important to qualify shielding calculations for ITER-like neutron environment for establishing confidence in the validity of the calculations. The Tokamak Fusion Test Reactor (TFTR) has started high power D–T operations and has produced copious yields of D–T neutrons. Previously, there have been attempts to directly characterize neutron spectra around TFTR [1,2]. However, there were large statistical uncertainties on the experimental measurements owing to poor counting statistics due to low intensity of D–T neutron source used. Later, extensive measurements were made with various electronic, film badge, TLD, etch track, and activation foil detectors to map the biological doses from test cell walls out to the first property line, during high power D–D discharges [3–5].

The D–T campaign of TFTR began with trace tritium shots in November 1993. Later, it was followed with higher power D–T discharges [6]. The availability of high D–T fusion neutron yields during TFTR high power D–T operations provides a useful opportunity to characterize tokamak shielding–penetration geometries of potential interest to ITER. These types of measurements can provide direct experimental data on the degree of enhancement of transmitted neutron flux along or across a realistic penetration, and, as such, can be used to validate calculational methods and to meet fusion reactor licensing requirements. The enhancement of neutron streaming in the shielding penetrations has the following significant consequences from the ITER viewpoint: (a) increased radiation damage to plasma

Elsevier Science S.A.
*SSDI* 0920-3796(94)00374-2

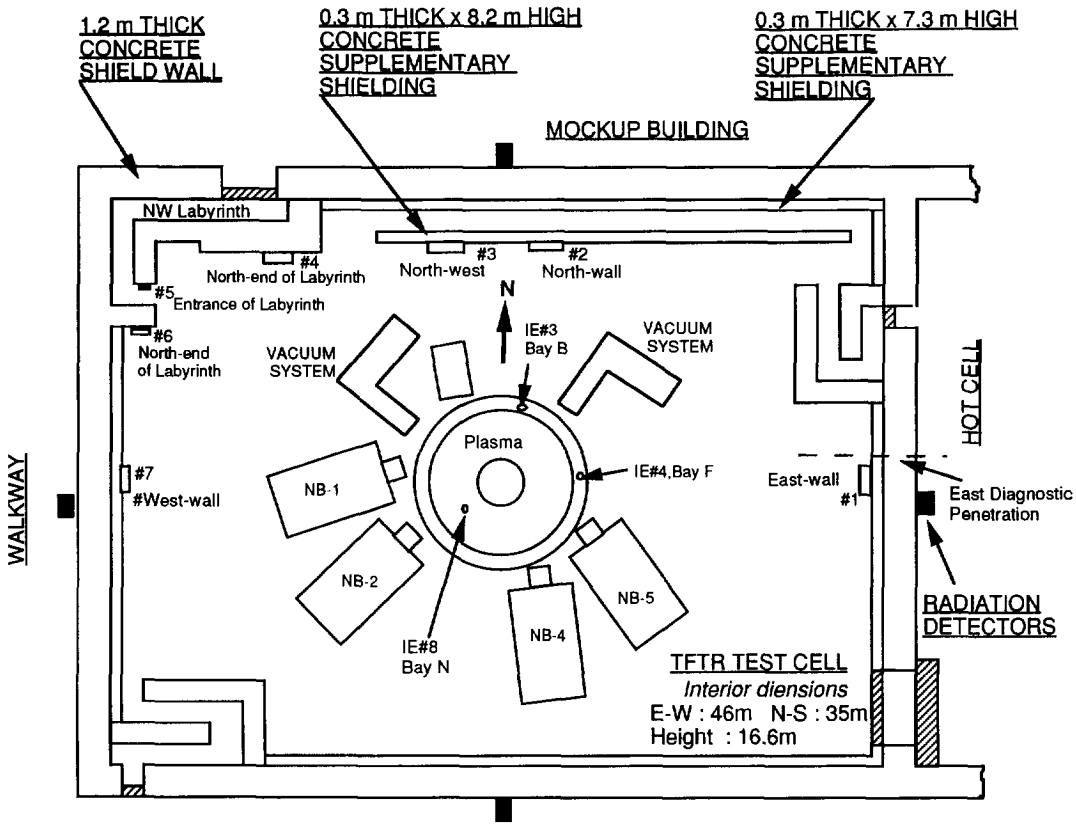


Fig. 1. A qualitative and simplified sketch of locations of foil boards on inner walls of TFTR test cell. The locations are marked as 1 (east wall) to 7 (west wall), including three locations to characterize the north-west labyrinth. Also shown is measured radioactivity for IE 8 that is closest to the TFTR plasma.

diagnostics–detectors, (b) increased biological dose rates behind the shield, and (c) increased radiation damage to superconducting magnets on outboard side.

TFTR has penetrations of different varieties inside the vacuum vessel, the test cell, and the adjoining hot cell. In the initial stage, we have chosen to characterize three different types of penetrations in and around the TFTR test cell: (1) a straight hollow pipe coming out of test cell concrete wall on east side of test cell into the hot cell, (2) a bent pipe coming out of test cell through north concrete wall, and (3) a labyrinth in north-west end of the test cell. The experimental measurements will consist of (i) neutron spectrum characterization near the vacuum vessel, (ii) neutron spectrum characterization around the chosen penetrations, and (iii) $\gamma$ and n dose measurements near and around the penetrations. Activation foils, film badges, and Bonner sphere techniques have been used for these measurements. The present paper focuses on characterization of neutron energy spectra near three sets of penetrations as mentioned above. The characterization of neutron energy spectrum near the vacuum vessel forms subject of a companion paper [7]. $\gamma$ and n dose measurements near the labyrinth were also conducted [8].

The measurements of induced radioactivity were done near the plasma and vacuum vessel, as well as on the inner walls of TFTR test cell. The induced radioactivity measurements were conducted for samples of aluminum, silicon, titanium, vanadium, chromium, iron, cobalt, nickel, copper, zinc, zirconium, niobium, molybdenum, indium, tungsten, and gold at various spectral locations during November 1993 through March 1994 period at TFTR. In this paper, we will be presenting and discussing measurements on inner walls of TFTR test cell.

## 2. Experiments

During D–T operations, TFTR discharges occur about 10–20 min apart. High D–T neutron yields occur during the 1 s, neutral deuterium or tritium beam heating of the discharges which last about 4 s. A given experimental day of D–T operations will include many D–D discharges for tuning and reference purposes. The irradiations close to plasma were performed on November 22, 1993, and February 24, 25 and 28, 1994 [7]. The irradiations on TFTR cell walls were performed on February 24 and February 28, 1994, during an entire day in each case. Fig. 1 provides a qualitative, but highly simplified, sketch of numbered locations (1–7) of irradiated foils on east (one location), north (two locations), and west (one location) inner walls of the TFTR test cell. The figure also shows north-west labyrinth and its three walls, i.e. north end, entrance, and west end, where foils were placed. In addition, this figure shows locations of three different irradiation ends (IEs) or terminal locations of the transport system that were used. These ends are much closer to plasma. Foils irradiated in the re-entrant location IE 8 are at a major radius of 2.58 m and 1.039 m above the midplane [7]. Re-entrant end IE 8 extends in from a racetrack flange on top of the vacuum vessel. It sees the hardest neutron energy spectrum with its proximity to the plasma (it represents the only irradiation end that falls within the nuclear boundary). IE 4 and IE 3 are located outside the vacuum vessel in the midplane of two different toroidal "bays" between TF coils. IE 4 is located 407.6 cm in major radius and 7.6 cm below the actual midplane in bay F. IE 3 is at a similar position somewhat above the midplane in bay B.

At each of the seven locations on test cell walls, an identical set of foils was irradiated. In addition, packs of radiation badges were also irradiated at the same locations. Out of every set, each foil was taped inside one of an array of widely spaced approximately 20 mm diameter and approximately 5 mm deep holes created on a 10 mm thick polystyrene board. A typical foil had a diameter of about 18 mm and thickness of 1 mm, but a gold foil was only 0.025 mm thick. A polystyrene board typically measured anywhere from 50 cm ×

Table 1
Observed radioactive products for foils irradiated on inner walls of TFTR test cell

| Foil | Irradiation day (shots' type) | Product and half-life | Foil | Irradiation day | Product and half-life |
|---|---|---|---|---|---|
| Ti | February 28, 1994 (D–T and D–D) | 43.7 h $^{48}$Sc, 3.34 days $^{47}$Sc | Zr | February 28, 1994 (D–T and D–D) | 72 m $^{97}$Nb, 16.9 h $^{97}$Zr, 78.4 h $^{89}$Zr, 64 days $^{95}$Zr |
| V | February 28, 1994 (D–T and D–D) | 43.7 h $^{48}$Sc | | February 24, 1994 (D–D) | None |
| Cr | February 28, 1994 (D–T and D–D) | 27.7 days $^{51}$Cr | Nb | February 28, 1994 (D–T and D–D) | 10.2 days $^{92m}$Nb |
| Fe | February 28, 1994 (D–T and D–D) | 2.58 h $^{56}$Mn, 312.2 days $^{54}$Mn | Mo | February 28, 1994 (D–T and D–D) | 66 h $^{99}$Mo, 10.2 days $^{92m}$Nb |
| Co | February 28, 1994 (D–T and D–D) | 70.8 days $^{58}$Co, 5.27 years $^{60}$Co | W | February 28, 1994 (D–T and D–D) | 23.9 h $^{187}$W |
| Ni | February 28, 1994 (D–T and D–D) | 70.8 days $^{58}$Co, 271 days $^{57}$Co | | February 24, 1994 (D–D) | 23.9 h $^{187}$W |
| Cu | February 28, 1994 (D–T and D–D) | 12.7 h $^{64}$Cu | Au | February 28, 1994 (D–T and D–D) | 2.69 days $^{198}$Au |
| | February 24, 1994 (D–D) | 12.7 h $^{64}$Cu | | February 24, 1994 (D–D) | 2.69 days $^{198}$Au |
| Zn | February 28, 1994 (D–T and D–D) | 12.7 h $^{64}$Cu, 13.8 h $^{69m}$Zn, 244.1 days $^{65}$Zn | | | |

50 cm to 50 cm × 100 cm. This arrangement ensured that the foils stayed firmly in place and that there was minimal self-shielding of neutron flux for a foil. Each of these boards was either hung or taped to the wall to keep it firmly in place.

Seven foil boards were left for irradiation during entire day of D–D discharges on February 24, 1994. Each board had four foils: copper, zirconium, tungsten and gold. There were a total of 47 neutron-yielding discharges. The first 15 discharges had relatively low yields. The average time between two successive discharges was 21.0 min. The total source neutron yield per discharge differed from discharge to discharge, varying from $2.13 \times 10^{13}$ to $7.07 \times 10^{13}$. Next five discharges had high yields. The total source neutron yield per discharge varied from $1.38 \times 10^{16}$ to $1.62 \times 10^{16}$. The mean spacing between two discharges was 16.3 m. The D–T neutron fraction ranged from 9.3% to 10.9%. Next three discharges had low yields. Last 24 discharges had high yields, with average spacing being 17.6 m. The total source neutron yield per discharge went from $9.51 \times 10^{15}$ to $1.38 \times 10^{16}$. The D–T neutron fraction was quite stable and ranged from 11.3% to 12.8%. The $\gamma$ spectroscopy of the activated foils was done at neutron activation (NA) laboratory of TFTR. The activated foils could only be removed in early morning of the following day owing to the short-lived activation in the test cell immediately following high power operations. Owing to limited counting time available, all the four foils on each board were removed and stacked in a single "rabbit" [7,9–11]. A "rabbit" is a hollow, cylindrical capsule that is made of polyethylene and has following dimensions: outer diameter, 2.54 cm; inner diameter, 1.91 cm; length, 6.35 cm. Also, it has a threaded cap on one end. In all, seven identical rabbits of four foils each were made and counted on one of the two HPGe detectors. The cooling times ranged from 10 h 51 min to 14 h 16 min, and each rabbit was counted only for an hour.

On February 28, 1994, again seven foil boards were irradiated. However, this time, each board had 13 foils: titanium, vanadium, chromium, iron, cobalt, nickel, copper, zinc, zirconium, niobium, molybdenum, tungsten, and gold. There were 29 discharges in all. The first 12 discharges were all D–D with average spacing between two successive discharges being 31.4 m. The total source neutron yield per discharge differed from discharge to discharge, varying from $4.04 \times 10^{12}$ to $1.04 \times 10^{16}$. The D–T neutron fraction ranged from 0.8% to 10.1%. Next six discharges were alternately D–T and D–D. The last 11 discharges were all D–T with average spacing being 30.5 m. The total source neutron yield per discharge differed again from discharge to discharge, varying from $3.38 \times 10^{16}$ to

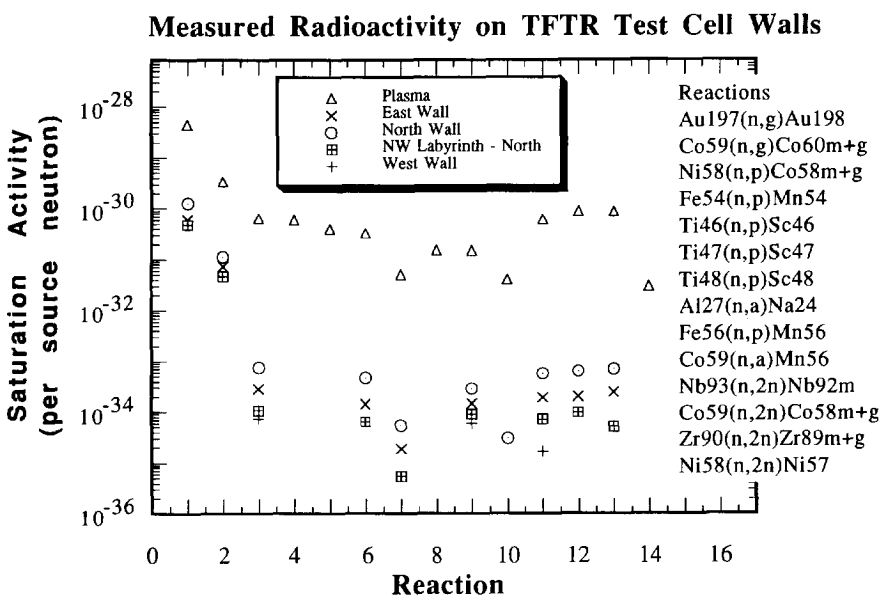


Fig. 2. Measured saturation activity per TFTR source neutron per target atom on inner walls of TFTR test cell for radioactive products of dosimetric reactions. Also shown is measured radioactivity for IE 8 that is closest to the TFTR plasma.

$7.89 \times 10^{17}$. The D–T neutron fraction was quite high and ranged from 75.1% to 93.5%.

γ spectroscopy of each foil was carried out using HPGe detector and data acquisition system at the PPPL Radiological and Environmental Measurements Laboratory. Each foil was counted directly and individually, and as many times as possible to measure all detectable radioactivities. The cooling times logged so far in this elaborate counting campaign range from 11 h 26 min to 58 days 11.7 h. It needs to be stressed that total number of foils counted in this campaign is 91, which is a large number for a single HPGe detector.

## 3. Treatment of raw data

The count spectra collected at NA Laboratory, for February 24 irradiations, and at REML, for February 28 irradiations, were analyzed using the corresponding peak-search analysis packages. Each analysis provided counts for each analyzed γ peak and its standard deviation. These peak counts were then processed to obtain, among other results, saturation activity for all radioactive isotopes of interest. The γ detector efficiency data, together with associated errors, for various calibration energies were provided by REML, and were used to obtain efficiency–energy fitting curves and covariant matrices by using least-squares minimization techniques. Due account of pulsed mode of TFTR operation was taken while processing the counts' spectra for all radioactive products, through different, customized programs for the two sets of irradiations. Decay γ yields and isotopic fractions were respectively adopted from table of radioactive isotopes [12] and table of isotopes [13]. The isotopic half-lives were adopted from Ref. [14]. For rabbit counting at NA Laboratory, calculation of current γ self-shielding for each γ peak became very important because of the presence of as many as four foils in a single rabbit. Considerable effort was invested in obtaining net correction factors that take into account changes in absolute detector efficiency as well as γ self-shielding for all γ rays emitted by each foil in a counted rabbit, as mentioned in Ref. [7]. The self-shielding correction factors for the REML countings were relatively easy to compute but were obtained, however, by the same procedure [7].

Regarding experimental error estimation, it is to be recognized that a number of parameters affect counting statistics. The primary parameters include neutron flux, half-life of γ emitter, detector efficiency, cooling time, counting time, activation cross-section and atom density. Sum-peak corrections also add up to the error. Obviously, it is impossible to give a single figure for even one sample material. For large majority of the experimental measurements, the error lies between about 5% and about 20%.

## 4. Discussion of measured activities

γ peak energies, γ yields, and half-lives for all the observed products for all the irradiated foils are readily available in Ref. [14]. We would be identifying each observed isotopic product through its name and half-life only. In what follows, we present brief discussion on various aspects of interest to both ITER and additional experimental campaigns at TFTR.

### *4.1. Measured saturation activities*

Extensive data have been obtained for practically all materials of interest. This database could be used variously by different users. Apart from its direct use for characterizing neutron energy spectra at various walls of TFTR test cell, it could be invaluable in testing and adjusting three-dimensional (3D) models of TFTR. In addition, these data would be of potential interest during regulatory licensing of ITER for qualifying activation calculations for similar situations in ITER. For example, one could expect the spectra at the test cell walls to resemble qualitatively those at the superconducting magnets of ITER. In what follows, we will appraise the status on saturation activities measured in various materials. Once saturation activities are known, it is straightforward to obtain decay–γ and other source terms required for decay–heat and/or biological dose calculations.

Material-wise observed products are listed in Table 1. As can be seen, only three activities could be measured following February 24, 1994, D–D neutron irradiation, i.e. 12.7 h (half life) $^{64}$Cu (from Cu foil), 23.9 h $^{187}$W (from W), and 2.69 days $^{198}$Au (from Au foil). It is noted here that, in all probability, as a result of the predominance of very large and overpowering Compton continuum caused by various peaks of $^{187}$W (from W), peaks from products of other materials, especially Zr, were totally submerged and, thus, were not observed for any of the seven rabbits. On the contrary, all the products listed in Table 1 were measured following February 28, 1994, irradiation (D–T plus D–D shots). Material-wise observed products were as follows: (1) Ti, 43.7 h $^{48}$Sc, 3.34 days $^{47}$Sc; (2) V, 43.7 h $^{48}$Sc; (3) Cr, 27.7 days $^{51}$Cr; (4) Fe, 2.58 h $^{56}$Mn, 312.2 days $^{54}$Mn; (5) Co, 70.8 days $^{58}$Co, 5.27 years $^{57}$Co; (6) Ni, 70.8 days $^{58}$Co, 271 days

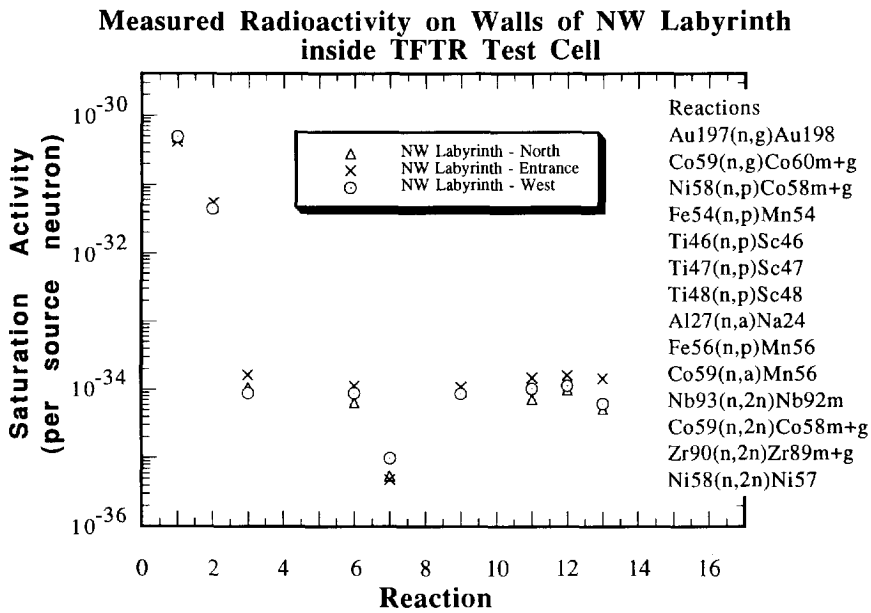


Fig. 3. Measured saturation activity per source neutron per target atom on three inner walls of north-west labyrinth inside TFTR test cell for radioactive products of dosimetric reactions. The walls are identified as north-west labyrinth north, entrance, and west.

$^{57}$Co; (7) Cu, 12.7 h $^{64}$Cu; (8) Zn, 12.7 h $^{64}$Cu, 13.8 h $^{69m}$Zn, 244.1 days $^{65}$Zn; (9) Zr, 72 min $^{97}$Nb, 16.9 h $^{97}$Zr, 78.4 h $^{89}$Zr, 64 days $^{95}$Zr; (10) Nb, 10.2 days $^{92m}$Nb; (11) Mo 66 h, $^{99}$Mo, 10.2 days $^{92m}$Nb; (12) W, 23.9 h $^{187}$W; (13) Au, 2.69 days $^{198}$Au.

### 4.2. Saturation activities for TFTR test cell walls

In Fig. 2, saturation activity per source neutron per target atom is shown for various dosimetric reaction products. For comparison, we have also included measured data for re-entrant irradiation end, say IE 8. It is simply marked as "plasma" on the figures to follow. This location is closest available location to burning plasma of TFTR and, as a result, provides largest and hardest neutron flux [7]. Note that all threshold reactions' activities are normalized to one D–T source neutron, whereas all capture reactions' activities are normalized to a TFTR source neutron (D–T + D–D). The reactions and their products include (1) $^{197}$Au(n,γ)$^{198}$Au, (2) $^{59}$Co(n,γ)$^{60m+g}$Co, (3) $^{58}$Ni(n, p)$^{58m+g}$Co, (4) $^{54}$Fe(n,p)$^{54}$Mn, (5) $^{46}$Ti(n,p)$^{46}$Sc + $^{47}$Ti(n,n'p or d)$^{46}$Sc + $^{48}$Ti(n,n'd or t)$^{46}$Sc, (6) $^{47}$Ti(n,p)$^{47}$Sc + $^{48}$Ti(n,n'p or d)$^{47}$Sc + $^{49}$Ti(n,n'd or t)$^{47}$Sc, (7) $^{48}$Ti(n,p)$^{48}$Sc + $^{49}$Ti(n,n'p or d)$^{48}$Sc + $^{50}$Ti(n, n'd or t)$^{48}$Sc, (8) $^{27}$Al(n,α)$^{24}$Na, (9) $^{56}$Fe(n, p)$^{56}$Mn, (10) $^{59}$Co(n,α)$^{56}$Mn, (11) $^{93}$Nb(n,2n)$^{92m}$Nb, (12) $^{59}$Co(n,2n)$^{58m+g}$Co, (13) $^{90}$Zr(n,2n)$^{89m+g}$Zr, and (14) $^{58}$Ni(n,2n)$^{57}$Ni. The reactions on abscissa of Fig. 2 are roughly arranged in the order of increasing effective neutron energy threshold, except for first two reactions that are capture reactions. Note that each reaction is assigned a number, e.g. $^{197}$Au(n,γ)$^{198}$Au, is assigned value of 1 on horizontal axis of Fig. 2. Only a single target atom is to be understood as assigned to each of these twelve radioactive products and they are respectively as follows: (1) $^{197}$Au, (2) $^{59}$Co, (3) $^{58}$Ni, (4) $^{54}$Fe, (5) $^{46}$Ti, (6) $^{47}$Ti, (7) $^{48}$Ti, (8) $^{27}$Al, (9) $^{56}$Fe, (10) $^{59}$Co, (11) $^{93}$Nb, (12) $^{59}$Co, (13) $^{90}$Zr, and (14) $^{58}$Ni. Note that, for some reaction products, the measured data for some wall locations are not available. The largest saturation activities occur for the two capture reactions, i.e. $^{197}$Au(n,γ)$^{198}$Au, and $^{59}$Co(n,γ)$^{60m+g}$Co, and clearly signal strong presence of thermal and as well as other low energy neutrons. Interestingly, one can easily mark the closeness of the data for all the locations for these products. On the contrary, there is a very large dispersion in the data for the reactions with thresholds, and the saturation activity varies from about $10^{-35}$ to about $10^{-33}$ per target nucleus for the walls. The largest values are almost two to three orders of magnitude lower than those for the plasma. The lowest saturation

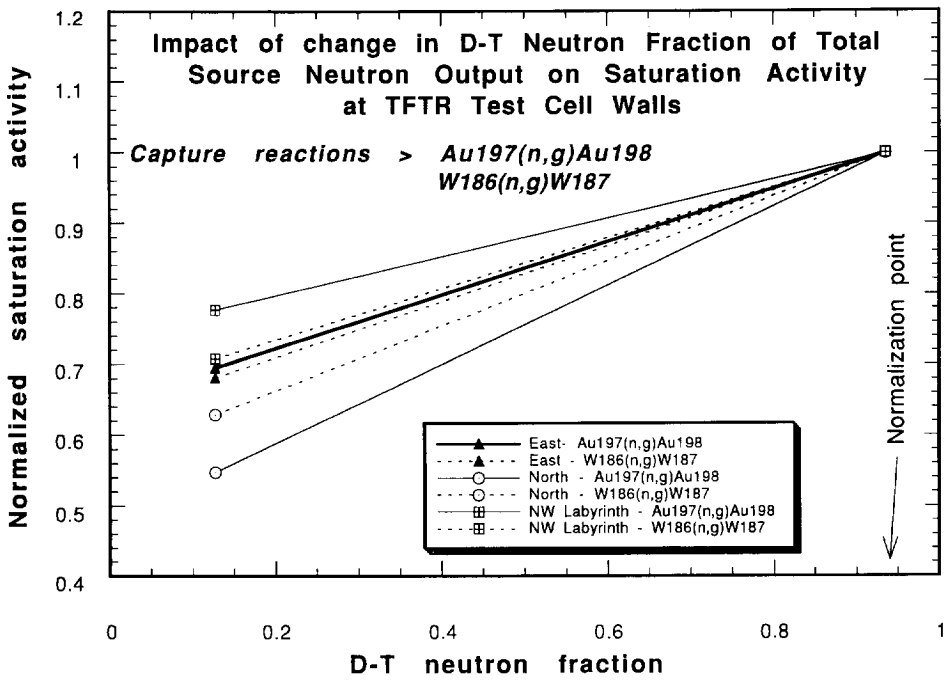


Fig. 4. Impact of change in D–T neutron fraction of a TFTR source neutron on saturation activity due to capture reactions at inner walls of TFTR test cell. Results for two radiative producers, i.e. $^{187}W$ (from W) and $^{198}Au$ (from Au) are shown for north wall, east wall, and labyrinth north-west entrance.

activity is observed for $^{48}Sc$, and the largest for $^{198}Au$.

As for comparison of saturation activities for different walls, it is obvious that the largest and the smallest activities are respectively seen for the north and the west walls of the test cell. At least, there are two contributing factors for such large differences: (1) direct flight path length for neutrons from plasma to the detector site, and (2) material composition, and effective optical path length for neutrons leaving the plasma on their way to the detector site. Of course, the scattering from other materials contributes too. The material arrangement in TFTR test cell around the plasma is far from being symmetric, and, in addition, the direct path lengths from plasma to the seven detector sites differ too.

### 4.3. Saturation activities for north-west labyrinth walls

In Fig. 3, saturation activity per source neutron per target atom is shown for various dosimetric reaction products for three walls of north-west labyrinth, i.e. north, entrance, and west walls (see Fig. 1). Again, the largest saturation activities occur for the two capture reactions, i.e. $^{197}Au(n,\gamma)^{198}Au$, and $^{59}Co(n,\gamma)^{60m+g}Co$. It is to be noted that $^{198}Au$ activity is almost 4 orders of magnitude larger than an average threshold activity. Also, almost all the largest activities pertain to "entrance" wall of the labyrinth. The saturation activities for all the threshold reaction products stay below $3 \times 10^{-33}$ per target nucleus. As mentioned earlier, the lowest and the largest saturation activities are observed for respectively $^{48}Sc$ and $^{198}Au$. "North" wall of the labyrinth has the lowest activities of its three walls.

## 5. Spectral information

### 5.1. Impact of D–T neutron fraction

Looking closely at saturation activity data for various reactions during TFTR D–D or D–T discharges with varying contribution of D–T neutrons, we learn that capture reaction products reveal noticeable dependence on D–T neutron fraction. Fig. 4 shows saturation activities for two capture reactions, i.e. $^{186}W(n,\gamma)^{187}W$, and $^{197}Au(n,\gamma)^{198}Au$, as a function of averaged

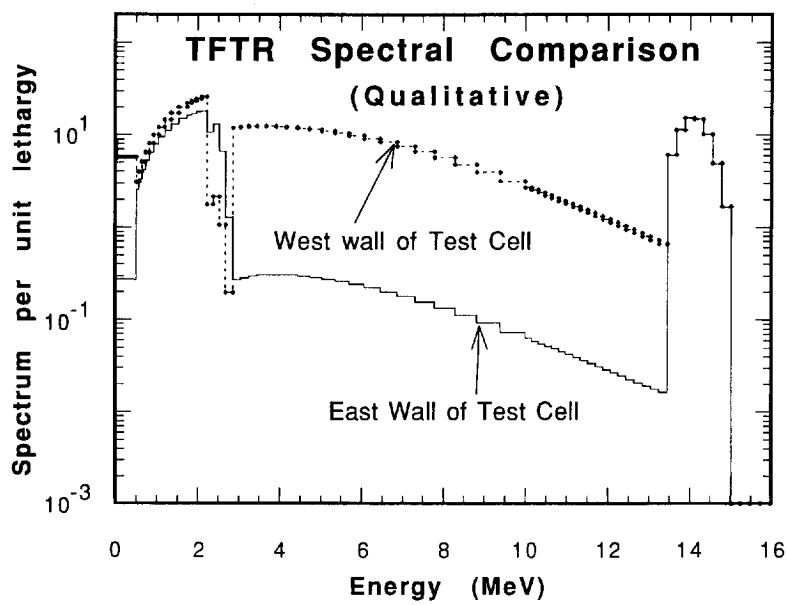


Fig. 5. Qualitative comparison of unfolded spectra for east and west inner walls of TFTR test cell.

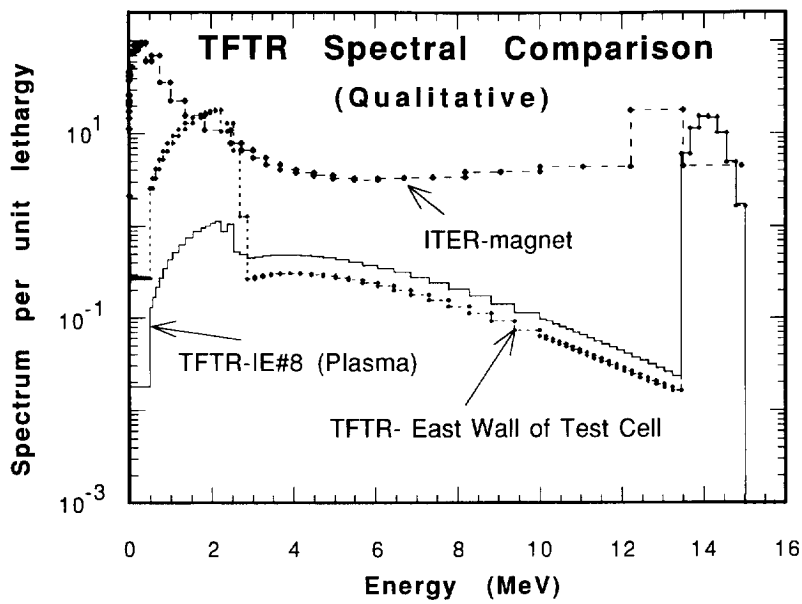


Fig. 6. Comparison of normalized spectra per unit lethargy for superconducting magnet of ITER, i.e. ITER magnet (self-cooled Li–V blanket option), first-wall kind of spectrum of IE 8 of TFTR (TFTR-IE 8), and east inner wall of TFTR test cell. Each spectrum is normalized such that there is 1 n $cm^{-2}$ (i.e. 1 D–T n $cm^{-2}$) in energy range 13.5–15 MeV.

D–T neutron fraction over all the discharges during the day for three of the walls. Note that each saturation activity has been normalized to its value at D–T neutron fraction of about 0.93 (February 28, 1994, irradiation). Up to about 50% change in saturation activity is seen as D–T neutron fraction goes up from about 12%

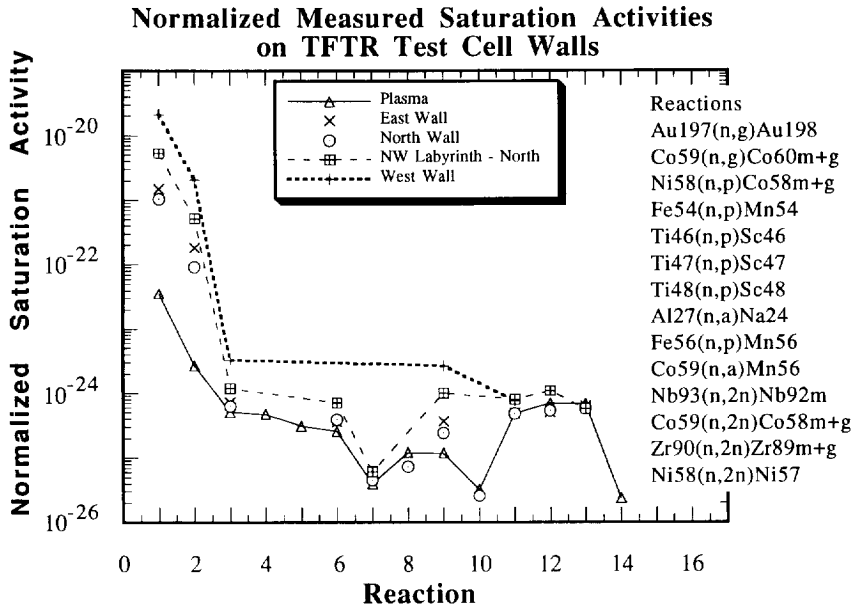


Fig. 7. Comparison of normalized, measured, saturation activities on inner walls of ITER test cell. The normalization is done to 1 D–T n $cm^{-2}$ for the measured saturation activity.

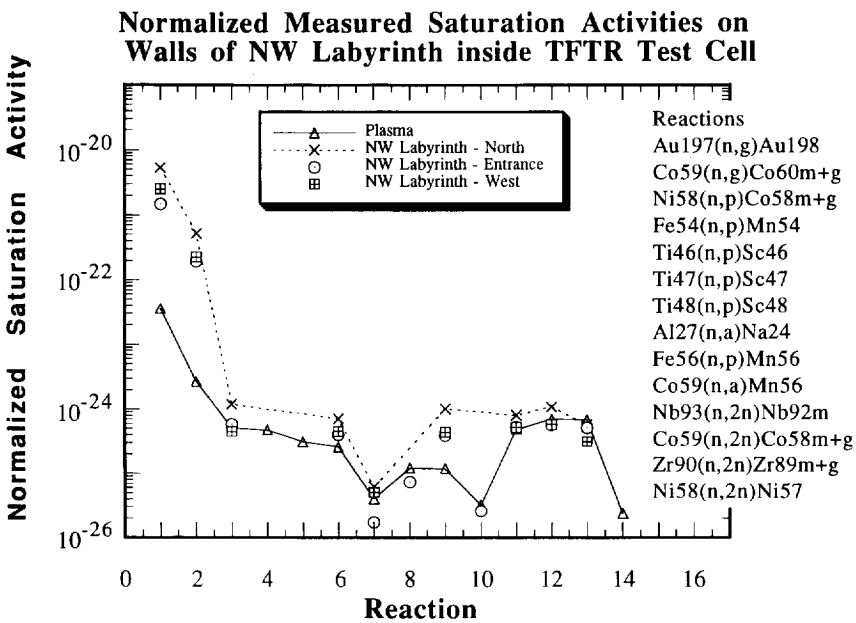


Fig. 8. Comparison of normalized, measured, saturation activities on three inner walls of north-west labyrinth inside TFTR test cell for radioactive products of dosimetric reactions. The walls are identified as NW labyrinth north, entrance, and west. The normalization is done to 1 D–T n $cm^{-2}$ for measured saturation activity.

Table 2
Neutron dose equivalents obtained for select locations on inner walls of TFTR test cell

| Location on inner walls of TFTR test cell | Neutron dose equivalent obtained from unfolded spectra for high power D–T discharges on February 28, 1994 (mrem (source neutron)$^{-1}$) [a] |
|---|---|
| East wall | $2.53 \times 10^{-13}$ (13%) |
| North to center east | $1.66 \times 10^{-12}$ (14%) |
| North, center west | $6.30 \times 10^{-13}$ (14%) |
| North-west labyrinth north | $1.42 \times 10^{-12}$ (15%) |
| North-west labyrinth entrance | $4.20 \times 10^{-13}$ (14%) |
| North-west labyrinth west | $1.04 \times 10^{-13}$ (11%) |
| West wall | $3.42 \times 10^{-14}$ (13%) |

[a] Values in parentheses represent one standard deviation error on neutron dose equivalent.

to about 93%. Thus, one could infer that worth of a D–T neutron to low end of neutron energy spectrum is as much as about 50% larger than that of a D–D neutron, close to inner walls of TFTR test cell. We have observed a similar trend for IE 8 (plasma) [7].

### 5.2. Spectral unfolding

It is natural to explore a possibility of unfolding neutron energy spectrum for various irradiation ends as a good number of measured, saturation activities are available for most of the locations. It is, however, apparent from the discussion in the preceding subsection that one has to contend with many parameters, in addition to usual problems associated with any unfolding code. Among others, D–T neutron fraction appears to impact saturation activity values, at least those resulting from neutron capture reactions. Another crucial parameter is input neutron energy spectrum required by most of the unfolding codes. This input guess has to be rather close to the real spectrum, an unknown, to obtain any meaningful output from these codes [15–17]. An extensive effort was invested in unfolding neutron energy spectra. The details of this effort will be published in another publication that will also include additional improvements. Fig. 5 compares unfolded neutron energy spectra for east and west walls of the test cell. It is to be noted that the spectra have been normalized to 1 D–T n cm$^{-2}$ in the energy range from 13.5 to 15 MeV. West wall spectrum appears to be considerably softer. This may be due to the extensive scattering and attenuation provided by the neutral beam line in that direction.

### 5.3. A spectral comparison of relevance to ITER

Fig. 6 compares three spectra. Each spectrum has been normalized to 1 D–T n cm$^{-2}$. The neutron spectrum for ITER, say ITER magnet, is for superconducting magnet of self-cooled Li–V blanket option under extensive studies at a time [18]. The spectrum for water-cooled design is also available and it is quite comparable with that included in Fig. 6 [18]. The other two spectra correspond to IE 8 (plasma) and east wall of TFTR test cell. One can observe that although there are differences in the spectra for ITER magnet and TFTR east wall in entire energy range, the spectral shapes are broadly comparable for all practical purposes.

### 5.4. Normalized, saturation activities on TFTR test cell walls

The unfolded spectra for all the locations are used to obtain individual integrated D–T neutron flux between 13.5 and 15 MeV. This integrated number is then used to obtain normalized saturation activities for 1 D–T n cm$^{-2}$. Fig. 7 compares normalized, saturation activities for the TFTR test walls. It can be inferred that the hardest neutron energy spectrum occurs for the north wall of the cell. On the contrary, the softest spectrum exists for the west wall. Interestingly, the spectrum for the north wall appears to be as hard as that for the plasma in most of the threshold reaction region, say between about 3 and about 15 MeV. The north direction between the tokamak and the north wall has relatively little intervening material, whereas, as noted above, the west wall is shielded by a neutral beam line.

### 5.5. Normalized, saturation activities on north-west labyrinth walls

Fig. 8 compares normalized, saturation activities for the three walls of the north-west labyrinth. The figure also shows the data for IE 8 (plasma) for reference. It can be inferred that the hardest neutron energy spectrum occurs for the "entrance" wall of the labyrinth. The softest spectrum exists for the "north" wall of the labyrinth.

## 6. Dose equivalents

As discussed in the previous section, the neutron energy spectrum at low end of the energy critically depends on the D–T neutron fraction of the total source neutron yield. In addition, the fraction of neutrons at the low end of the energy spectrum is quite large for all seven locations. This clearly means that the dose equivalent will have strong contributions from low energy neutrons. Note that the neutron fluence to dose equivalent factor rises by a factor of about 60 only in the range from a thermal to 14 MeV neutron [19]. Table 2 summarizes the measured neutron dose equivalents. Using the unfolded spectra, we estimate the dose equivalents to vary from about $3.4 \times 10^{-14}$ mrem (TFTR neutron)$^{-1}$ for west wall to about $1.7 \times 10^{-12}$ mrem (TFTR neutron)$^{-1}$ for the north wall of the TFTR test cell. These values are much larger than those given for D–D neutrons in Refs. [4] and [5]. There, the range for west wall was given as $1.14 \times 10^{-15}$–$2.03 \times 10^{-14}$ mrem (TFTR neutron)$^{-1}$ [4,5]. The range provided for the north wall was $1.66 \times 10^{-14}$–$4.11 \times 10^{-14}$ mrem (TFTR neutron)$^{-1}$. Thus, we observe, using these two sets of dose equivalents for the inside of the north wall, that the neutron dose equivalents for a D–T discharge (present case) are about 15–100 times those for a D–D discharge. Interestingly, this range of ratio compares favorably with a value of about 20, as predicted in Ref. [20], for neutron dose equivalent outside the TFTR test cell north wall. Even though we cannot directly compare the calculated ratio with the experimental range (given above) for obvious reasons, we learn, however, that "worth" of a D–T neutron could be much larger than that of a D–D neutron, in contributing to neutron dose equivalent, in certain situations. Note that there have been a number of changes in material arrangements in TFTR test cell vis-à-vis older experiment by Hajnal and colleagues [5]. The locations for our experiment differ from those reported in Ref. [5]. Also, the standard deviation on the measured activities in Ref. [5] varied from about 35% to about 64%. As mentioned above, the standard deviation on the measured activities in the present work is in the range 5%–20% only for most of the dosimetric activities. In addition, the hardest neutron energy covered in Ref. [5] was 5 MeV.

As a note of caution, it will be our endeavor in near future to reproduce the preliminary dose equivalent results with additional experiments, measurements, and analysis before finalizing the dose equivalents for all the locations reported in this paper.

## 7. Conclusions

Extensive measurements of fusion neutron induced radioactivity in various materials of interest to ITER were carried out beginning with first D–T shots in November 1993 at TFTR. The measurements were done at various irradiation ends close to plasma, as well as on seven locations on inner walls of TFTR test cell. Three of these locations pertained to three different walls of north-west labyrinth of the test cell. For the locations on the cell walls, the saturation activities were measured for various products of titanium, vanadium, chromium, iron, cobalt, nickel, copper, zinc, zirconium, niobium, molybdenum, tungsten, and gold. Clear differences were observed in saturation activities for various walls of the test cell, especially for threshold reactions. The largest saturation activities were determined for the north wall, whereas the lowest activities were detected for the west wall of the test cell. As for the north-west labyrinth, its "entrance" wall had the largest activities, whereas its "north" wall had the least activities.

The measured saturation activities for dosimetric reactions were unfolded to obtain the neutron energy spectra. The unfolded spectra were utilized to compare qualitatively the spectra for the TFTR test cell walls with those for superconducting magnet of an ITER design. In spite of the differences, the spectral shapes are inferred to be broadly similar. Also, the unfolded spectra were used to obtain normalized activities for 1 D–T n cm$^{-2}$. It was found that the neutron energy spectrum incident on north wall is as hard as that for the TFTR plasma (IE 8) between about 3 and about 15 MeV. As for the north-west labyrinth, its "north" wall has the softest spectrum, whereas its "entrance" wall has the hardest spectrum. The dose equivalents for all the seven locations were also estimated using the unfolded spectra. The dose equivalents vary from $3.4 \times 10^{-14}$ mrem (TFTR neutron)$^{-1}$ for west wall to $1.7 \times 10^{-12}$ mrem (TFTR neutron)$^{-1}$ for the north wall

of the TFTR test cell. These values are one to two orders of magnitude larger than those given for D–D neutrons in an earlier work [5]. The major reasons for such a large difference might be the dominance of D–T neutrons in the present work as well as large errors on measured activities in the referenced work. Further investigation of the difference is necessary before any conclusions as to its implications are drawn.

## Acknowledgments

Authors are grateful to D. Birckbichler and the staff of the PPPL REML for their technical assistance. Thanks are also due to Cris W. Barnes of LANL and James Eggleston of UCLA for their help. This work was supported in part by US DOE Contracts DE-AC02-76-CHO3073 and DE-FG03-86ER52123.

## References

[1] R.T. Santoro, J.M. Barnes, R.G. Alsmiller Jr. et al., Comparisons of calculated and measured spectral distributions of neutrons from a 14-MeV neutron source inside the tokamak fusion test reactor, Fusion Technol. 11 (1987) 420–428.

[2] J.K. Dickens, J.W. McConnell, K.M. Chase et al., Measurements of the neutron and gamma-ray fluences in the TFTR test cell due to a point source simulating D–T fusion plasma neutron production, Fusion Technol. 12 (1987) 270–280.

[3] H.W. Kugel, C.W. Barnes, J. Gilbert et al., Measurements of TFTR radiation shielding during high power D–D operations, Fusion Technol. 19 (1991) 1989–1995.

[4] H.W. Kugel et al., TFTR radiation contour and shielding efficiency measurements during D–D operations, Fusion Technol. 26 (1994) 963–972.

[5] F. Hajnal, N. Azziz, K. Decker et al., Measurement of the neutron radiation fields at the Princeton tokamak fusion test reactor (TFTR), Final Rep., 1991.

[6] J.D. Strachan et al., Fusion power production from TFTR plasmas fueled with deuterium and tritium, Phys. Rev. Lett. 72 (1994) 3526.

[7] A. Kumar, M.A. Abdou, H.W. Kugel, C.W. Barnes and M.J. Loughlin, Radioactivity measurements of ITER materials using TFTR D–T neutron field, Fusion Eng. Des. 28 (1995).

[8] H. Kugel, G. Ascione, S. Elwood et al., Measurements of TFTR D–T radiation shielding efficiency, Fusion Eng. Des. 28 (1995).

[9] E.B. Nieschmidt, Analysis programs and standardization of the neutron activation system at TFTR, Rev. Sci. Instrum. 57 (8) (1986) 1757–1759.

[10] E.B. Nieschmidt et al.., Calibration of the TFTR neutron activation system, Rev. Sci. Instrum. 59 (8) (1988) 1715–1717.

[11] C.W. Barnes et al., Operation and cross calibration of the activation foil system on TFTR, Rev. Sci. Instrum. 61 (10) (1990) 3190–3192.

[12] E. Browne and R.B. Firestone, in V.S. Shirley (ed.), Table of Radioactive Isotopes, Wiley–Interscience, New York, 1986.

[13] C.M. Lederer and V.S. Shirley, Table of Isotopes, Wiley, New York, 7th edn., 1978.

[14] A. Kumar, Y. Ikeda, M.A. Abdou, M.Z. Youssef, C. Konno, K. Kosako, Y. Oyama, T. Nakamura and H. Maekawa, Induced radioactivity measurements in fusion neutron environment: joint report of USDOE/JAERI collaborative program on fusion neutronics, Reps. UCLA-ENG-91-32/UCLA-FNT-53 and JAERI-M-93-018, February 1993.

[15] F.G. Perey, STAY'SL: least squares dosimetry unfolding code system, RSIC computer code collection PSR-113, March 1984.

[16] A. Kumar, Source normalization in least-squares dosimetry unfolding, Trans. Am. Nucl. Soc. 47 (1984) 155.

[17] F.B.K. Kam, SAND II: neutron flux spectra determination by multiple foil activation—iterative method, RSIC computer code collection CCC-112, June 1975.

[18] H.Y. Khater, personal communications to A. Kumar, March 23, 1994, and June 1, 1994.

[19] A.E. Profio, Radiation Shielding and Dosimetry, Wiley–Interscience, New York, 1978, p. 328.

[20] L.P. Ku and S.L. Liew, A semi-empirical algorithm for determining radiation field characteristics in TFTR, in Proc. 8th Int. Conf. on Radiation Shielding, Arlington, TX, April 24–28, 1994.